Multi-chord observation of stellar occultation by the near-Earth asteroid (3200) Phaethon on 2021 October 3 (UTC) with very high accuracy

Fumi Yoshida [1,2,*] Tsutomu Hayamizu,[3] Kazuhisa Miyashita,[4,5] Hiroyuki Watanabe,[5,6] Hidehito Yamamura,[7] Hiroshi Akitaya,[2] Akira Asai,[5] Yasunori Fujiwara,[5,8] Tateki Goto,[9] George L. Hashimoto,[10] Akitoshi Hatanaka,[11] Toshihiro Horaguchi,[12] Miyoshi Ida,[5] Kazuyoshi Imamura,[13] Ken Isobe,[5,8] Masateru Ishiguro,[14] Noboru Kaizuka,[15] Hisashi Kasebe,[5,8] Yohei Kawasaki,[16] Taewoo Kim,[17] Katsuhiko Kitazaki,[5,18] Norihiro Manago,[5] Masafumi Matsumura,[19] Hiroshi Matsushita,[20] Shuji Matsuura,[21] Takahiro Nakamura,[22] Toshihiro Nagata,[7] Hirotomo Noda,[23] Masaaki Ogawa,[24] Osamu Ohshima,[25] Minoru Owada,[5] Kazuyuki Saitou,[26] Mitsunori Tsumura,[27] Yoshihiro Ueyama,[24] Hayato Watanabe,[5] Masa-yuki Yamamoto,[28] Hideki Yoshihara,[5] Takao Fujiwara,[10] Miyu Haraguchi,[10] Hironori Hayashi,[21] Tomoya Hitotsuda,[29] Toshihiro Horikawa,[9] Kai Ishida,[21] Tadashi Ito,[8] Sunho Jin,[14] Wonseok Kang,[17] Toshihiko Katayama,[9] Koji S. Kawabata,[30] Ryosuke Kawasaki,[31] Kihyeon Kim,[14] Masayuki Kita,[9] Naoko Kitazaki,[18] Hiroya Kurisu,[11] Makoto Matsushima,[32] Chika Matsumi,[21] Ayami Mihari,[13] Masaru Naka,[11] Tatsuya Nakaoka,[30] Reiko Nishihama,[32] Yukio Nishiyama,[33] Sadao Nukui,[29] Masahiko Oba,[34] Takaya Okamoto,[2] Yujiro Omori,[35] Jinguk Seo,[14] Hiroki Shirakawa,[9] Tomoshi Sugino,[20] Yuki Tani,[28] Kazuhiko Takagaki,[29] Yukikazu Ueda,[8] Seitaro Urakawa,[36] Masanari Watanabe,[37] Kouhei Yamashita,[33] Misato Yamashita,[10] Isao Sato,[6] Shosaku Murayama,[9] Tomoko Arai,[2] David Herald,[6] and Arika Higuchi[38]

[1] University of Occupational and Environmental Health, Japan, 1-1 Iseigaoka, Yahata, Kitakyusyu, Fukuoka 807-8555, Japan

[2] Planetary Exploration Research Center, Chiba Institute of Technology, 2-17-1 Tsudanuma, Narashino, Chiba 275-0016, Japan

[3] Saga Hoshizora Astronomy Center, 328 Nishioka-cho, Oaza Takataro, Saga, Saga 840-0036, Japan

[4] Japan regional Coordinator for Lunar Occultation observation (JCLO), Japan

[5] Japan Occultation Information Network (JOIN), Japan

[6] International Occultation Timing Association (IOTA), PO Box 20313, Fountain Hills, AZ 85269-0313, USA

[7] NPO KWASAN ASTRO NETWORK, c/o Kwasan Observatory, 17-1 Kitakazan-ohmine-cho, Yamashina-ku, Kyoto, Kyoto 607-8471 Japan

[8] Japan Astronomical Club, 2-16-8 Mikunihonmachi, Yodogawa, Osaka, Osaka 532-0005, Japan

[9] Museum of Astronomical Telescopes, 30-1 Sukemitsu-Higashi, Tawa, Sanuki, Kagawa 769-2306, Japan

[10] Okayama University, 3-1-1 Tsushimanaka, Kita, Okayama 700-8530, Japan

[11] Kumano Astronomical Club, Kumano, Mie, Japan

[12] National Museum of Nature and Science, 4-1-1 Amakubo, Tsukuba, Ibaraki 305-0005, Japan

[13] Anan Science Center, 8-1 Nagakawa Kamifukui Minami-Kawabuchi, Anan, Tokushima 779-1243, Japan

[14] Seoul National University, 1 Gwanak-ro, Gwanak-gu, Seoul 08826, South Korea

[15] ASCOMI, Kuwana, Mie 511-0821, Japan

[16] Astronomical Club FUKUYAMA, Fukuyama, Hiroshima, Japan

[17] National Youth Space Center, Jeollanam, Deokheung yangjjokgil 200, Goheung 59567, South Korea

[18] Nakano Stargazers Club Japan

[19] Faculty of Education and Center for Educational Development and Support, Kagawa University, Saiwai-cho 1-1, Takamatsu, Kagawa 760-8522, Japan

[20] Shima, Mie 517-0604, Japan

[21] Kwansei Gakuin University, 1 Uegahara, Gakuen, Sanda, Hyogo 669-1330, Japan

[22] Kitakyusyu Sirius-kai, Kitakyusyu, Fukuoka 803-0864, Japan

[23] National Astronomical Observatory of Japan, National Astronomical Observatory of Japan, 2-12 Hoshigaoka, Mizusawa, Oshu, Iwate 023-0861, Japan

[24] Nippon Meteor Society, Japan

[25] Okayama University of Science, 1-1 Ridaicho, Kita-ku, Okayama-shi, Okayama 700-0005, Japan

[26] Nichihara Astronomical Observatory, Makurase, Tsuwano, Kanoashi, Shimane 699-5207, Japan

[27] Wakayama, Wakayama 640-0351, Japan

[28] Kochi University of Technology, 185 Miyanokuchi, Tosayamada, Kami City, Kochi 782-8502, Japan

[29] Aridagawa Town Astronomy Club, Aridagawa-cho, Arida-gun, Wakayama, Japan

[30] Hiroshima Astrophysical Science Center, Hiroshima University, 1-3-1 Kagamiyama, Higashi-Hiroshima, Hiroshima 739-8526, Japan

[31] Kougominami, Nishiku, Hiroshima, Hirosima 733-0823, Japan

[32] Kinokawa Astronomy Club, Kinokawa, Wakayama, Japan

[33] Astronomical Society of Shikoku, Takamatsu, Kagawa 761-0321, Japan

[34] Mitsubishi Heavy Industries, Kure, Hiroshima 737-8508, Japan

[35] Fujii Gakuen, 1-3-1 Shinhama, Marugame, Kagawa 763-0063, Japan

[36] Japan Spaceguard Association, Bisei Spaceguard Center, 1716-3 Okura, Bisei, Ibara, Okayama 714-1411, Japan

[37] Nagoya University, Furo-cho, Chikusa-ku, Nagoya, Aichi 464-8601, Japan

[38] Kyoto Sangyo University, Motoyama, Kamigamo, Kita-ku, Kyoto, Kyoto 603-8555, Japan

*E-mail: fumi-yoshida@med.uoeh-u.ac.jp

Abstract

We observed a stellar occultation by (3200) Phaethon, which occurred in western Japan on 2021 October 3 (UTC). This observation was requested by the DESTINY$^+$ mission team, which plans to conduct a flyby of asteroid Phaethon in 2028. Overall, this research effort contributes towards a large-scale observation campaign with a total of 72 observers observing from western Japan to southern Korea. 36 stations were established, and stellar occultation by the asteroid Phaethon was detected in 18 of them. This is the first time that this many multiple chord observations have been made for such a small asteroid (it has a diameter of 5–6 km). Observational reductions show that the apparent cross-section of Phaethon at the time of the occultation could be approximated using an ellipse with a major diameter of 6.12 ± 0.07 km and a minor diameter of 4.14 ± 0.07 km, and a position angle of $117°\!.4 \pm 1°\!.5$. As can be seen from the small error bars of the fitted ellipse, we have succeeded in estimating the shape and size of the asteroid with an

extremely high degree of accuracy. Our observation results, together with other observations, will be used to create a 3D model of Phaethon and to improve its orbit. The instruments that we used for this observation are commonly used by many amateur astronomers in Japan for occultation observations and are not difficult to obtain. This paper describes the method and results of our observations using a CMOS camera and a GPS module, so that many people can participate in occultation observations in the future.

1 Introduction

The asteroid (3200) Phaethon is an Apollo-type near-Earth asteroid that orbits the Sun with an orbital period of 1.43 yr. Its semimajor axis is 1.27 au and the orbit shape is elongated and tilted from the ecliptic plane with an eccentricity of 0.89 and an inclination of $22°.3$. The thermal history of Phaethon has been studied by many researchers and its surface temperatures have been estimated (Ohtsuka et al. 2009; Jewitt & Li 2010; Jewitt et al. 2019; MacLennan et al. 2021). According to those studies, Phaethon's surface temperature can reach approximately 1000 K with a perihelion distance of 0.14 au from the Sun, located inside Mercury's orbit. In contrast, with an aphelion distance of 2.40 au, the surface temperature of Phaethon reaches approximately 200 K.

Thus, Phaethon's surface experiences extreme temperature fluctuations, approximately 800 K, throughout the orbital period of 1.43 yr. Such extreme and periodic changes efficiently metamorphose the surface of Phaethon, resulting in Phaethon's surface seeming to be covered with materials created by thermal processes. Such objects are rarely seen among the near-Earth asteroids.

Phaethon is assumed to be the parent body of the Geminid meteor shower, which is observed every December (Gustafson 1989; Williams & Wu 1993; Jenniskens 2006). Phaethon is classified as a B- or F-type asteroid (Borisov et al. 2018; Kareta et al. 2018; Lazzarin et al. 2019; Lee et al. 2019; Tabeshian et al. 2019; Ohtsuka et al. 2020; Lin et al. 2020), which belong to the C-complex asteroid type, like (162173) Ryugu (containing carbon, organic matter, and water metamorphic minerals; Watanabe et al. 2019). Therefore, the dust ejected from Phaethon, including particles of the Geminid meteor shower, is thought to contain carbon and organic matter, which are precursors of life. These precursors are brought to Earth every year through Geminid meteor showers. Therefore, by studying the asteroid Phaethon, we can investigate the composition of the organic dust supplied to Earth and the mechanism of dust emission from asteroids.

Given these characteristics, Phaethon warrants further investigation. Hence, the Institute of Space and Astronautical Science (ISAS) of the Japan Aerospace Exploration Agency (JAXA), in collaboration with the Planetary Exploration Research Center of the Chiba Institute of Technology, is planning to send a spacecraft to Phaethon through a project called "DESTINY$^+$" (Demonstration and Experiment of Space Technology for INterplanetary voYage with Phaethon fLyby and dUst Science) (Arai 2021; Arai et al. 2021a, 2021b). The goal of DESTINY$^+$ is to conduct a scientific investigation of the asteroid Phaethon and its dust using more advanced ion engine navigation and multi-object flyby exploration technologies. The launch of the spacecraft is scheduled for 2024. The DESTINY$^+$ spacecraft will first be injected into a long elliptical orbit around the Earth by an Epsilon launch vehicle. It will then undergo "spiral orbit raising" to gradually increase its orbital altitude, which will take approximately two years. Subsequently, it will leave the Earth through a "lunar swing-by" and gradually change its orbit over a period of approximately two years to reach the flyby point with Phaethon in early 2028. During this period (∼4 yr), the spacecraft will observe interstellar and interplanetary dust using a DESTINY$^+$ dust analyzer (DDA) (Krüger 2021; Li et al. 2021) onboard the spacecraft. For the flyby phase, the DESTINY$^+$ spacecraft will approach Phaethon within a distance of 500 km, and the asteroid will be observed using two onboard cameras: a telescopic camera for Phaethon (TCAP) and a multi-band camera for Phaethon (MCAP) (Ishibashi et al. 2021; Hong et al. 2021). In addition, the DDA will directly analyze the dust around Phaethon. After the Phaethon flyby, the DESTINY$^+$ mission team will consider a flyby of the asteroid (155140) 2005UD, thought to be a breakup object from Phaethon, based on their similarity in orbit (Ohtsuka et al. 2006).

The DESTINY$^+$ spacecraft will orbit almost on the ecliptic plane, waiting for Phaethon to approach, and will encounter Phaethon at a speed of 36 km s^{-1} during the

flyby. At such a high flyby speed, the spacecraft will remain in the vicinity of Phaethon for only a short time; hence, there will be no time to conduct a detailed investigation of the asteroid once the spacecraft is close to it. Therefore, it is essential to study the characteristics, such as shape, albedo, and rotation period of the object, in as much detail as possible before the flyby and to consider the exposure time, angle of view of the two cameras, and flyby timing to ensure the success of the mission.

In 2017 December, Phaethon approached Earth at approximately 0.07 au and brightened to about 11 mag. Taking advantage of this opportunity, the DESTINY$^+$ science team called for Phaethon's worldwide observation campaign. Researchers responded to the call and made their own observations. As a result, together with previous studies, the rotation period of Phaethon and the direction of Phaethon's rotation axis (Pravec et al. 1998; Krugly et al. 2002; Ansdell et al. 2014; Hanuš et al. 2016, 2018; Kim et al. 2018), spectral type (Borisov et al. 2018; Kareta et al. 2018; Lazzarin et al. 2019; Lee et al. 2019; Tabeshian et al. 2019; Ohtsuka et al. 2020; Lin et al. 2020), etc., were determined with high accuracy. Radar observations made at the Arecibo Observatory have shown that the effective diameter of Phaethon is approximately 6 km (Taylor et al. 2019). Phaethon was found to have a spinning-top shape similar to that of (162173) Ryugu (Watanabe et al. 2019) and (101955) Benne (Lauretta et al. 2019), which were explored by Hayabusa2 (Watanabe et al. 2017) and OSIRIS-REx (Enos & Lauretta 2019), respectively.

Despite these intensive observations, the absolute magnitude essential for estimating the diameter of Phaethon could not be accurately determined. The absolute magnitude of the asteroid is defined as the *V* magnitude (visible) at a solar phase angle of $0°$; however, the relationship between Phaethon, the Sun, and Earth's orbit does not allow Phaethon to be observed at this solar phase angle. The minimum solar phase angle during the closest-approach period in 2017 was approximately $20°$. Therefore, large estimation errors still exist in the diameter and albedo of Phaethon. The DESTINY$^+$ mission team needed to estimate Phaethon's diameter by a different method rather than by using the absolute magnitude.

An alternative method of using absolute magnitude to determine the size of an asteroid is through occultation observation, which involves measuring the size of the shadow cast on the ground by an asteroid occulting a background star. This was the main method used to determine the diameter of asteroids until it became possible to calculate the diameter from the albedo estimated by combining absolute magnitude and infrared observations. Determining the asteroid's diameter via visible and infrared observations requires a thermal model, which involves some "rough

assumptions," culminating in systematic errors negatively impacting the accuracy at which the diameter can be determined. In contrast, as occultation observations directly measure the size of an asteroid's shadow, diameter estimation using this method is determined solely by the precision of the measurement of occultation timing. Therefore, high-precision observations can determine the diameter with high accuracy. Furthermore, the measurement of asteroid size with stellar occultation is more accurate than that with any other method available at the moment.

Thus, the DESTINY$^+$ science team decided to use occultation observations to obtain a more accurate estimate of Phaethon's diameter. The effective diameter of Phaethon, estimated by radar observations in 2017, was approximately 6 km (Taylor et al. 2019), and occultation observations for such a small object were almost unprecedented because the duration of occultation was very short (less than one second) and the orbits were often ill determined and consisted of large uncertainty. The smallest asteroid successfully observed occulting a star before 2019 was (11072) Hiraoka, with a diameter of 7 km, but only one observation site reported a positive detection (e.g., Tony George's report).[1] However, this situation has changed significantly in recent years. The Gaia Space Observatory of the European Space Agency (ESA) has cataloged the position, distance, and motion of stars with unprecedented accuracy (Gaia Collaboration 2016, 2018, 2021), and the All-Sky Survey (Catalina Sky Survey, Drake et al. 2009; PanSTARRS, Magnier et al. 2020) has worked on determining the orbits of even small asteroids.

As the accuracy of stellar positions improves and orbital information on many asteroids is gathered, predictions of more occultation events are becoming more accurate. In this context, one of the authors, Isao Sato, predicted stellar occultation by Phaeton in the western United States on 2019 July 29. Another author, Hirotomo Noda, also predicted that stellar occultations by Phaethon would be observed in Japan on 2019 August 21 and October 15. Therefore, the DESTINY$^+$ science team requested experienced occultation observers in Japan and abroad to observe these stellar occultations.

At the request of the DESTINY$^+$ science team, systematic observations of stellar occultation by Phaethon were conducted in the western part of the United States on 2019 July 29. Observation volunteers, located on 66 lines drawn at 680 m intervals from the center of the predicted occultation zone in the San Joaquin Valley, helped to observe the occultation of a star of apparent magnitude 7. Simultaneous observations were made at 19 points in Las Vegas.

[1] ⟨http://spiff.rit.edu/richmond/occult/hiraoka_may2006/Observation_of_a_Very_Small_Asteroid.doc⟩.
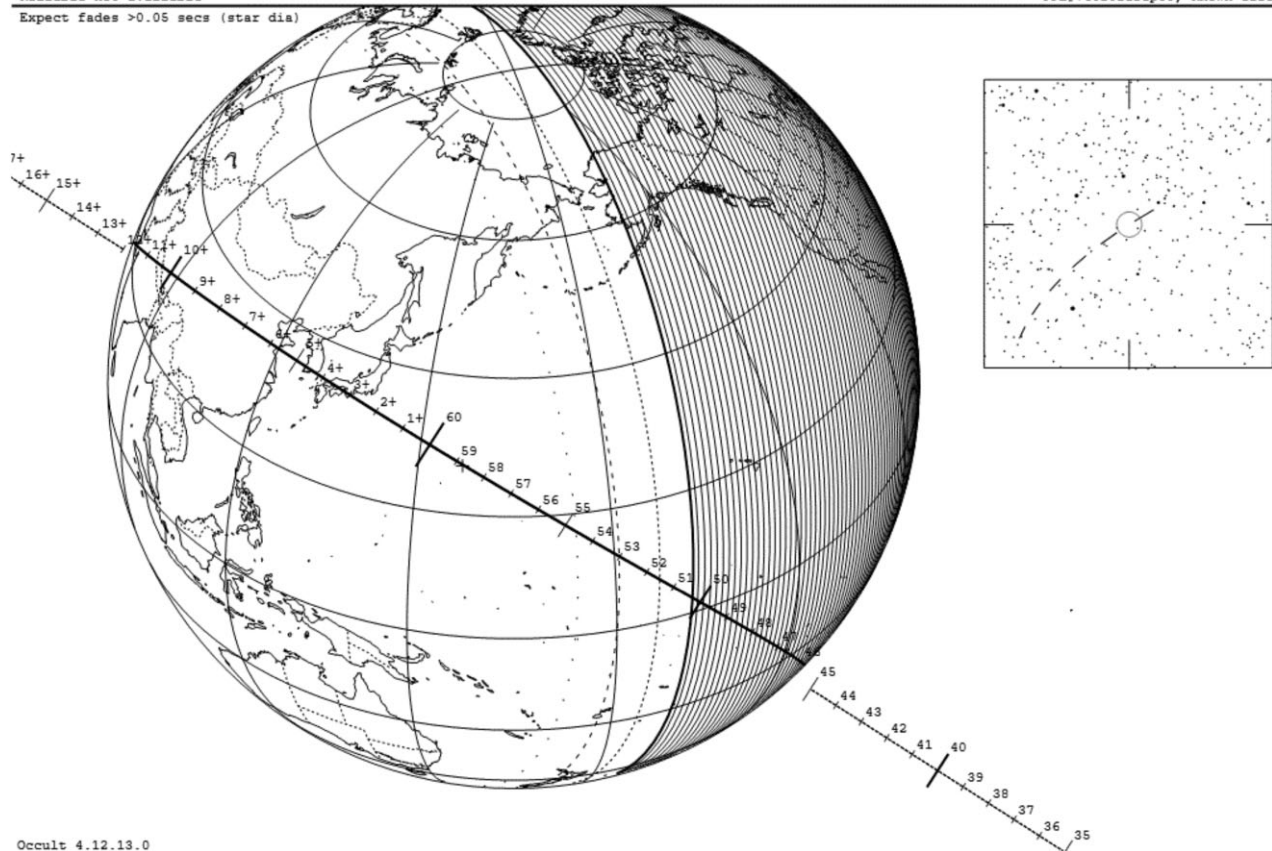
Fig. 1. Predicted occultation zone for Phaethon's stellar occultation on 2021 October 3 from Steve Preston's website. The shaded area is the daylight area. The dotted and dashed lines indicate the twilight zones. The occultation zone extends from the Kii Peninsula, Shikoku, and the Chugoku regions through the southern Korean Peninsula to China.

The results showed that Phaethon's shadow was slightly larger than a 5 km diameter circle. Stellar occultations by Phaethon were observed consecutively in California, USA, on 2019 September 29; Virginia, USA, on 2019 October 12; Algeria on 2019 October 15 and 25; and Mississippi, USA, on 2019 October 5. However, these observations did not provide sufficient data to improve the results obtained on 2019 July 29 due to the small number of observation points. These observations have been described and summarized in Dunham et al. (2019, 2020, 2021).

In Japan, observation parties consisting of amateur astronomers and planetary scientists observed Phaethon's occultation on 2019 August 21 (in Hokkaido) and October 15 (in Yamagata–Miyagi). On Hokkaido's Oshima Peninsula, 31 observers attempted to make observations from 16 different sites but were unfortunately unable to do so because of cloud cover. From Yamagata to Miyagi prefectures, 10 parties were ready for observation on 2019 October 15, but most of their observations were obstructed due to fog. Only two groups managed to capture the occultation by Phaethon in clear sites (Dunham et al. 2020).[2,3] Although stellar occultations by Phaethon were intensively observed in 2019 and 2020, these observations were not sufficient to determine the size of Phaethon with a relative uncertainty of less than 5%, the aim of the DESTINY+ mission team. The DESTINY+ science team called for another campaign to observe Phaethon's stellar occultation, which was visible in Japan on 2021 October 3 (UTC). This provided an opportunity to determine the size of Phaethon at a different angle from the stellar occultation event by Phaethon that occurred in the western part of the United States on 2019 July 29, thus providing a different cross-section.

In this paper, we describe the results of an observation campaign for the stellar occultation by Phaethon in western

---

[2] ⟨https://aas.org/sites/default/files/2020-10/David_Dunham_DPS52.pdf⟩.

[3] ⟨http://iota.jhuapl.edu/DunhamAstSciConf2019.ppt⟩.

Japan. The prediction of the occultation is described in section 2, and the observational methods are explained in section 3. Section 4 presents the analysis method and results, and section 5 summarizes the results and outcomes of observations, and provides future occultation prediction and observation plans.

2 Prediction

Detailed predictions for Phaethon's stellar occultation event in East Asia on 2021 October 3 (UTC) were provided by Steve Preston (International Occultation Timing Association, IOTA),[4] which was a response to Tsutomu Hayamizu, who noticed this event. According to this prediction, Phaethon would occult a 12.0 mag star in the Auriga constellation (UCAC4 646−021974 = GSC 2894−00131). This event can be observed along a path across Japan, Korea, and China at 16:58 (UTC) on 2021 October 3, as shown in figure 1. When the occultation occurs, the star dims 6.5 mag from the magnitude before and after occultation. The maximum occultation duration is 0.680 s. This prediction was made using the catalog of stars provided by the Gaia mission[5] and the Data Processing and Analysis Consortium (DPAC)[6] and the position of the asteroid based on the orbital information provided by the IAU Minor Planet Centre. The parameters related to this occultation event are listed in table 1, and the information on the star occulted is presented in table 2.

3 Observations

3.1 Instruments

As the star that Phaethon occulted on 2021 October 3 (UTC) has a magnitude of 12, we recommended that the observers in the observation campaign use a telescope with an aperture size of 25 cm or larger. However, if the sensitivity of the camera is very high and an observation system with a small F-number is constructed, a telescope with a smaller aperture could be used. In summary, it was possible to observe if one could devise a method to increase the amount of light received per pixel in the detector of the CMOS camera. In the observation system of one of the observers, a Schmidt–Cassegrain system with an F10 telescope was converted to an F2 class by stacking a 0.63× and 0.33× reducer, or F3 with a combination of a 0.63× reducer and 0.5× eyepiece reducer. A smaller F-number also has the advantage of providing a wider field of view, which makes it easier to identify a target star and select a star for

4   ⟨https://www.asteroidoccultation.com/2021_10/1003_3200_73168_Summary.txt⟩.

5   ⟨http://www.cosmos.esa.int/gaia⟩.

6   ⟨http://www.cosmos.esa.int/web/gaia/dpac/consortium⟩.

Table 1. Occultation prediction.

The event	
Date and approximate time	2021 Oct 3, 16:45–17:11 [UTC]
Geocentric midpoint	2459491.20748750 [JD]
Magnitude of the target star	12.03
Magnitude drop	6.51 [mag]
Estimated maximum duration	0.680 [s]
Occultation path	
Approximate projected width	6 [km]
1σ path widths	± 0.19 [km]
1σ timing	± 0.2 [s]
1σ of RA, Dec	(±0.001 [″], ±0.001 [″])
Approximate speed	7.9212 [km s^{-1}]
Asteroid's shadow	
General information for Phaethon	
Approximate physical diameter	5 [km]
Approximate angular diameter	0.004 [″]
Distance from the Earth	1.78770 [au]
Orbital information for Phaethon	
Orbit source	JPL#765
Date of fit	2021 Sept 30
Source of astrometry used	MPC, JPL
Orbital elements of Phaethon*	
Mean anomaly	206°.34845409
Argument of pericenter	322°.17813164
Longitude of node	265°.22132172
Inclination	22°.25640530
Eccentricity	0.88977584
Semimajor axis	1.27135638 au
Perihelion distance	0.14013419 au
Absolute magnitude	H = 14.32
Slope parameter	G = 0.15
Element epoch	MJD 59490.70748750 TDT (2021 Oct 3.7075)

*⟨https://ssd.jpl.nasa.gov/horizons/app.html⟩.

Table 2. Occultation star information.[†]

Designation	UCAC4 646−021974
RA (J2000.0)	04^{h}50^{m}35^{s}2052
Dec (J2000.0)	+39°05′11″251
Total mean error in the position (J2000.0)	24 [mas]
UCAC fitting model magnitude (579–642 nm)	12.357 [mag]
Proper motion in RA[*cos(Dec)]	−4.2 [mas yr^{-1}]
Proper motion in Dec	−1.9 [mas yr^{-1}]
2MASS J magnitude	9.402 [mag]
2MASS K_s magnitude	8.418 [mag]
B magnitude from APASS	14.678 [mag]
V magnitude from APASS	12.855 [mag]
r magnitude from APASS	12.162 [mag]
i magnitude from APASS	11.379 [mag]
Spectral type	K0[‡]

[†]From the VizieR catalog ⟨http://vizier.u-strasbg.fr/viz-bin/VizieR⟩.
[‡]From the observation by the 1.5 m Kanata Telescope, Hiroshima University with spectrometer HOWPol.

comparison. We did not use filters normally used in astronomical photometric observations. As the primary aim of occultation observations is to detect stellar dimming with a better S/N, it is better to collect more light. Therefore, no filter was required.

In this observation campaign, most observers used either the ZWO ASI290MM[7] or QHY174M-GPS[8] CMOS camera. The QHY174M-GPS camera has a built-in GPS receiver system; therefore, it is not necessary to perform the operations described in subsection 3.2 or the time correction using the 1 PPS LED emission described in section 4.

3.2 Recording method of the exact time

One of the most important aspects of observing stellar occultation by an asteroid is recording as accurately as possible when the target star is obscured by the asteroid and when it reappears. Various methods have been used to precisely record this timing. Herein, we describe the standard method currently used by most Japanese occultation observers using a complementary metal–oxide–semiconductor (CMOS) camera and a global positioning system (GPS) receiver.

CMOS cameras are rapidly becoming popular among Japanese occultation observers as alternatives to the analog video cameras commonly used for occultation observations. CMOS cameras are more sensitive than analog video cameras and can capture images at higher speeds. They are ideal for capturing videos of astronomical phenomena that last less than one second, such as asteroid occultations. However, the accuracy of timestamping using a computer that captures images is not always reliable. This is because a time delay occurs when the image captured by the CMOS camera is transmitted to the computer, which records the image data on the hard disk or other recording devices, depending on the processing power of the computer. This is a major problem when recording astronomical phenomena that last less than one second.

To solve this problem, we use a GPS module to precisely adjust the computer's system clock and then project the one pulse per second (PPS) emission of the light-emitting diode (LED) produced by the GPS module on to the image. We then measured the difference between the timestamp of the image taken by the computer and the timing of the 1 PPS LED emission by using a light curve of 1 PPS LED emission produced by taking images with a slightly shifted timing from the exact LED emission. We corrected the timestamp by adding or subtracting the difference to derive accurate occultation timing. We also read the subframe time using

the light curve of the 1 PPS LED emission and diffraction model.

Since the PPS only provides information on a rise time of one second, the computer's system clock has to be adjusted in advance to an uncertainty of less than 0.5 s relative to UTC. Therefore, we first adjusted the computer's system clock to the GPS time received by the GPS module, which identifies the observation location (latitude and longitude) and provides the time within an uncertainty of ±0.3 s to Japan Standard Time (or UTC). The free software "GPS Clock"[9] was released in Japan, runs on Windows 10/8/7, and automatically corrects the computer's system clock time to GPS time when installed on the computer. Most observers who participated in the occultation observation campaign obtained this software and a GPS module to ensure that the clock time of their computer was accurate and congruent with the GPS time during the observation. By using computer time information as accurate and detailed as the GPS time when observing the emission of the 1 PPS LED with the exposure time set to a value not divisible by an integer of 1 s, the timing of the start of the exposure gradually deviates from the timing of the 1 PPS LED emission. The light intensity of the 1 PPS LED emission captured in the image gradually changed over time. By capturing a series of such images over a certain period and plotting the changes in the light intensity, the start timing of the 1 PPS LED emission with respect to the frames can be determined. In our observation campaign, we captured such images for 30 s before and after the occultation event. This procedure allows the timestamp to be corrected in milliseconds (sections 3 and 4).

3.3 Image capture method

In order to ensure a uniform method of analysis, in this observation session, we asked observers to acquire images whenever possible using "SharpCap,"[10] which is an astronomical camera capture tool that runs on Windows 7–11 and supports a variety of cameras including the QHY and ZWO astronomical cameras. Among the observers, the SharpCap settings were unified as follows.

SharpCap setting

Format	Mode	: MONO8

Binning	: 2

Output Format	: AVI

Image Info	Time Stamp	: On

Camera Control	Frame Rate	: Max.

---

[7] ⟨https://astronomy-imaging-camera.com/product/asi290mm⟩.

[8] ⟨https://www.qhyccd.com/qhy174gps/⟩.

[9] ⟨https://www.vector.co.jp/soft/winnt/personal/se508988.html⟩.
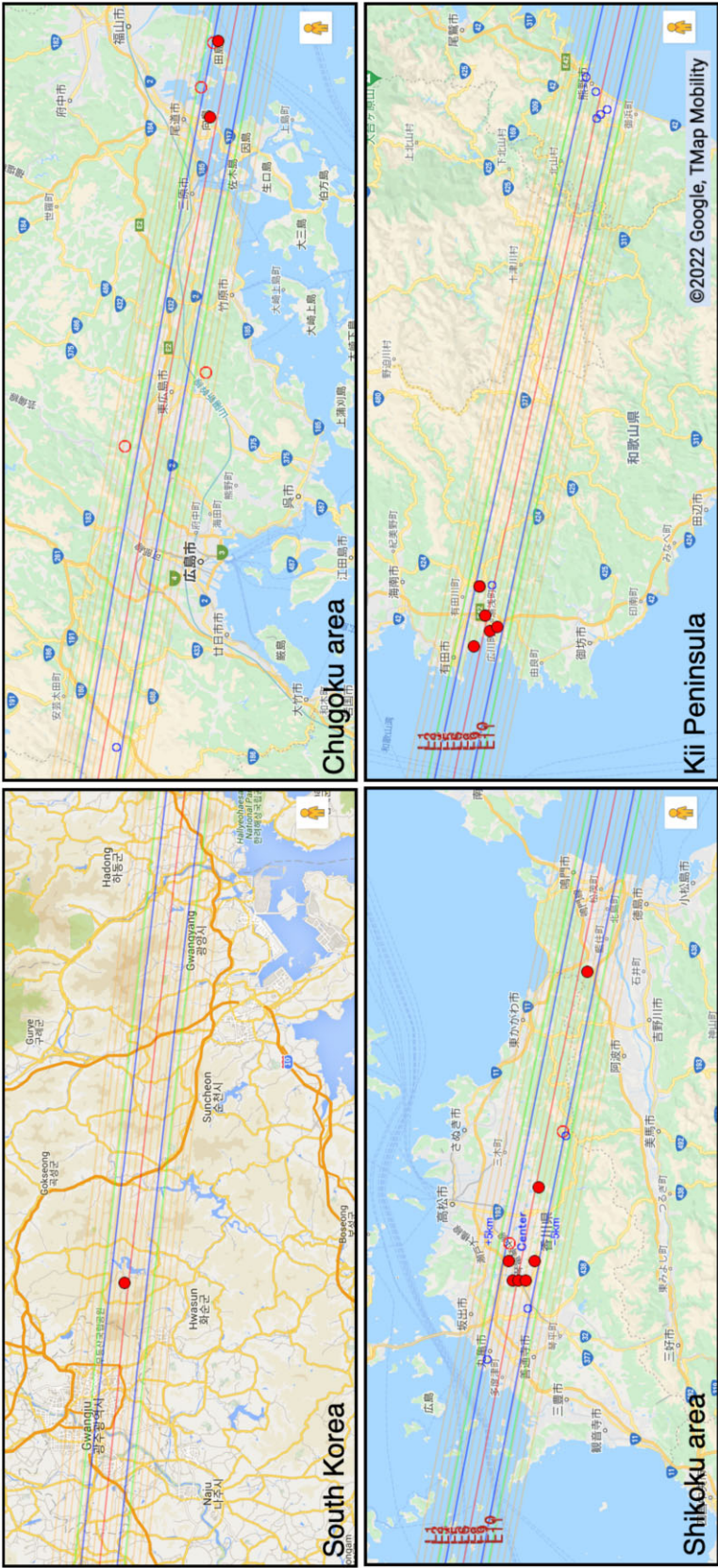
[10] ⟨https://www.sharpcap.co.uk⟩.

Fig. 2. Observation array. Lines (orange) are defined every 1 km from the center of the occultation zone (red line) in the width direction of these lines. The blue line is the north–south limit of the occultation zone and the green line is the 1σ-error range of the occultation zone. Red circles indicate sites of negative detection; Phaethon did not occult the target star. Blue circles indicate the locations where observations were unsuccessful due to bad weather or equipment malfunction. Top left: There is another observation site in Korea outside the map where detection is negative. Top right: In the Chugoku area of Japan, two sites had positive detections and four sites had negative detections. Bottom left: In the Shikoku area in Japan, the disappearance of the target star due to occultation by Phaethon was observed at seven observation sites, and no disappearance was observed at two observation sites. Lower right: On the Kii Peninsula in Japan, disappearance was observed at eight locations in the Wakayama Prefecture on the western side of the peninsula. Observers in Mie Prefecture on the eastern side of the Kii Peninsula were on standby under a cloudy sky, and no observations were made.

For cameras with cooling systems, the target temperature was set in addition to the settings described above. The output format was set to AVI because this can be read by the analysis software "Limovie."[11] In SharpCap, if "Time Stamp" is set to On, the time up to 1/1000 s is displayed at the top left of the image. Simultaneously, the time starting at 0:0:0:0 on 1 AD January 1 is written to the eight pixels in the top-left corner of each frame as 24 bit data in units of 100 ns. The time value for each frame is read by Limovie. In addition to these settings, the exposure time must also be set; however, the optimum value for the length of the exposure time was set by each observer, depending on the individual telescope.

3.4 Observation array

As shown in figure 1, the predicted occultation zone extended from the Kii Peninsula, Shikoku, and the Chugoku regions to southern Korea. Prior to the observation, 10 lines were set at intervals of 1 km from the center of the occultation zone to the north and south, and 72 observers who gathered in response to the call for the observation campaign were assigned. To reduce the risk of bad weather, the observers were placed in a wide region along the track, as shown in figure 2. As the orbit of Phaethon has already been well determined, observation points were densely set within the 1σ-error range of the occultation zone to accurately determine Phaethon's shape. In addition, some observation points were set beyond the 1σ-error range of the occultation zone. Since the target star was dark (12th magnitude), we asked observatories and schools with a 1 m class telescope close to the occultation zone to participate in this observation. In total, there were 36 observational data points.

The red line in figure 2 represents the center line of the predicted occultation zone. Light orange lines are drawn along the track of the occultation zone spaced 1 km from the red line. The blue lines are the north–south limits of the occultation zone and the green lines are the 1σ-error line of the occultation zone. The filled red circles indicate observation sites where occultation by Phaethon was detected. The red circles indicate observation sites where no occultation by Phaethon was detected (i.e., negative detection). Blue circles indicate sites where observations were unsuccessful because of weather or instrument malfunction.

Some observers near the northern and southern limits of the occultation zone detected occultation by Phaethon, while others did not, even though they were only approximately 400 m apart from each other. This implies that this

observation campaign obtained data that could constrain the shape of the northern and southern limits of Phaethon. Of the 36 observation sites, 18 were positive for detection and seven were negative.

The leader of each observation site was required to provide the following information: 1. names of the observers; 2. name of the observation site, latitude, longitude, and elevation of the observation site, and name of the geodetic system; 3. start and end times of the observation; 4. the detection/lack of detection of a disappearance; 5. the start and end times of the disappearance, if a disappearance was observed. 6. observation equipment; 7. time-keeping method; and 8. image data. The image data were uploaded and shared on the server provided to the observation team. Table 3 shows the location of each observation site (latitude, longitude, and elevation) and the observation equipment (telescope aperture, CMOS camera, exposure time, and time acquisition method) based on the reports from the leader of each observation site. The rightmost column in table 3 indicates whether the disappearance of the target star owing to occultation was observed. The letters indicate the following: P, disappearance observed (positive detection); N, passage (disappearance not observed, negative detection); F, instrument trouble/failure; C, no observation due to bad weather (clouded out).

4 Analysis method and results

The data from the 23 sites with positive and negative detections were mostly analyzed with Limovie. Although a disappearance was observed at observation sites No. 5 and No. 15, as shown in tables 3 and 4, the SETI/Unistellar Citizen science team performed this analysis, which was different from the analysis method described here.

The analysis method is shown below, using data taken from observation site No. 21 as an example. At observation site No. 21, a 0.424 s disappearance was observed. The frame of the AVI file loaded with Limovie is shown in figure 3a. This image was captured using SharpCap on a computer whose system clock was precisely set using a GPS module, as described in subsection 3.1. The date and time of image acquisition are shown on the top left of the image. The right edge of the image was brightened because the light from the 1 PPS LED emission produced by the GPS module was reflected in the image. The star occulted by Phaethon is indicated by the red circle. The light blue concentric circles represent the sky background specified for relative photometry of the target star.

First, the intensity variation of the 1 PPS LED emission, measured in the purple square in the center right of the

---

[11] ⟨https://astro-limovie.info/limovie/limovie_en.html⟩.

Table 3. Observation array.

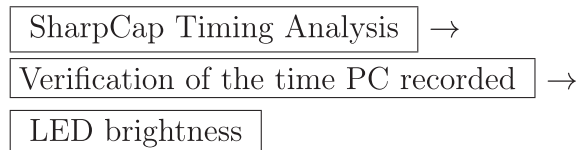| Obs. site	Observers	Longitude	Latitude	Alt. [m]	Tel. ap. [cm]	Camera	Exp. time [s]	Time keeping	Detection*
1	T. Hayamizu	+132°39′04″0	+34°29′28″5	226	28	ZWO ASI290MM	0.030328	GPS	N
2	Yoshida et al.	+133°15′38″5	+34°23′02″7	3	26	QHY174M-GPS	0.2	GPS	N
3	Hashimoto et al.	+133°20′08″4	+34°22′03″9	4	28	QHY174M-GPS	0.06	GPS	N
4	Ohsima et al.	+133°58′52″4	+34°15′42″8	58	25	ZWO ASI290MM	0.005	GPS	N
5	T. Goto	+135°14′55″9	+34°02′45″3	52	11	Sony IMX224	0.3	SETI†	P
6	Tsumura et al.	+135°14′56″1	+34°02′44″8	68	30	ZWO ASI290MM	0.0333	NTP‡	P
7	Manago et al.	+135°14′55″8	+34°02′44″4	68	50	ZWO ASI290MM	0.0227	NTP‡	P
8	Y. Kawasaki	+133°20′18″4	+34°21′38″8	3	28	ZWO ASI183MM Pro	0.0343	GPS	P
9	H. Noda	+133°57′01″8	+34°15′46″0	80	28	QHY174M-GPS	0.033	GPS	P
10	T. Nagata	+135°08′50″8	+34°03′14″8	2	35	ZWO ASI178MM	0.0312	GPS	P
11	H. Yoshihara	+133°12′31″2	+34°22′16″6	193	25	ZWO ASI290MM	0.0256	GPS	P
12	Yamamoto et al.	+133°55′3″2	+34°15′24″4	53	31	ZWO ASI183MM	0.0333	GPS	P
13	Ishiguro et al.	+127°04′46″1	+35°06′39″6	200	36	ZWO ASI174MM	0.059	GPS	P
14	M. Ida	+135°11′56″5	+34°02′14″6	28	28	ZWO ASI290MM	0.0502	GPS	P
15	H. Matsushita	+135°11′56″2	+34°02′13″8	98	11	Sony IMX224	0.3	SETI†	P
16	Isobe et al.	+133°55′02″6	+34°14′58″4	38	30	ZWO ASI290MM	0.0256	GPS	P
17	Kitazaki et al.	+134°04′30″4	+34°13′13″4	144	28	ZWO ASI290MM	0.0312	GPS	P
18	H. Yamamura	+135°10′22″5	+34°01′50″7	4	24	ZWO ASI290MM	0.0311	GPS	P
19	Fujiwara et al.	+133°55′05″6	+34°14′21″2	52	28	ZWO ASI390MM	0.0344	GPS	P
20	Imamura et al.	+134°26′28″7	+34°09′11″3	114	28	ZWO ASI290MM	0.0312	GPS	P
21	Hi. Watanabe	+135°10′47″9	+34°01′15″1	7	20	ZWO ASI290MM	0.0256	GPS	P
22	H. Kasebe	+133°57′02″9	+34°13′34″4	62	28	ZWO ASI290MM	0.0247	GPS	P
23	Horaguchi et al. (1)	+134°10′16″2	+34°11′11″3	325	60	WAT-910HX	0.033	GPS	N
24	Akitaya et al.	+132°46′37″1	+34°22′39″7	511	150	QHY174M-GPS	0.05	GPS	N
25	Kim et al.	+127°26′48″3	+34°31′34″7	81	100	ZWO ASI600MM	0.25	KRISS/UTCK	N
26	Ueyama et al.	+135°15′13″9	+34°01′32″1	109.8	20	ZWO ASI290MM	—	GPS	F
27	T. Nakamura	+132°08′42″5	+34°29′57″2	571	20	QHY174M-GPS	0.1	GPS	F
28	M. Ogawa	+133°52′27″5	+34°13′58″3	45.4	30	ZWO ASI224MC	0.0312	GPS	F
29	Horaguchi et al. (2)	+134°10′00″0	+34°10′47″6	310	25	QHY174M-GPS	—	GPS	F
30	Matsumura et al.	+133°47′15″9	+34°17′26″4	27	70	WAT-120N	0.03	GPS	F
31	K. Saitou	+131°50′20″9	+34°32′01″9	255	75	ZWO ASI183MC Pro	8	GPS	F
32	Kaizuka et al.	+136°03′08″9	+33°52′21″3	60	25	ZWO ASI290MM-cool	—	GPS	C
33	Asai et al.	+136°02′43″7	+33°52′43″8	190	45	ZWO ASI290MM	—	GPS	C
34	A. Hatanaka	+136°05′24″7	+33°52′47″8	17	40	ZWO ASI290MM	—	GPS	C
35	Ha. Watanabe	+136°06′55″9	+35°53′34″0	33	20	ZWO ASI290MM	—	GPS	C
36	M. Owada	+136°03′39″0	+33°51′48″7	52.6	25	ZWO ASI290MM	—	GPS	C

*"P" and "N" are positive detection and negative detection (miss), respectively. "F" is instrument failure or trouble. "C" means clouded out.
†Data analysis was done by the SETI/Unistellar Citizen science team.
‡GPS was not available.

image in figure 3a, was used to measure the delay/advance of the 1 PPS timestamp relative to UTC, using Limovie's "SharpCap Timing Analysis" function to validate the computer-recorded timestamps. Here is how this works: 1 PPS LED emission rises every second and lasts for 100 ms. By taking images with an exposure time in which the number of frames output per second is not an integer, the brightness of the 1 PPS LED emission increases or decreases at a constant rate. By examining this change in brightness, the frames near the light emission can be identified; the

frames are shown by blue and red points in figure 3b. On the Limovie screen,

$$\boxed{\text{SharpCap Timing Analysis}} \rightarrow$$
$$\boxed{\text{Verification of the time PC recorded}} \rightarrow$$
$$\boxed{\text{LED brightness}}$$

produces a graph of the intensity variation of the 1 PPS LED emission measured in the purple square (figure 3b). The start time of the 1 PPS emission, which is represented

Table 4. Results from the positive detections.

Obs. site	Observers	Disappearance (UTC)	Uncertainty [s]	Reappearance (UTC)	Uncertainty [s]	Duration [s]	Length of chord [km]*
5†	T. Goto	$17^{\rm h}03^{\rm m}08^{\rm s}\!.98$	0.18	$17^{\rm h}03^{\rm m}09^{\rm s}\!.43$	0.18	0.45	3.565±1.426
6	Tsumura et al.	$17^{\rm h}03^{\rm m}09^{\rm s}\!.012$		$17^{\rm h}03^{\rm m}09^{\rm s}\!.261$		0.249	1.972
7	Manago at al.	$17^{\rm h}03^{\rm m}09^{\rm s}\!.016$		$17^{\rm h}03^{\rm m}09^{\rm s}\!.266$		0.25	1.980
8	Y. Kawasaki	$17^{\rm h}03^{\rm m}29^{\rm s}\!.3$		$17^{\rm h}03^{\rm m}29^{\rm s}\!.54$		0.24	1.901
9	H. Noda	$17^{\rm h}03^{\rm m}22^{\rm s}\!.848$	0.011	$17^{\rm h}03^{\rm m}23^{\rm s}\!.090$	0.011	0.242	1.917±0.087
10	T. Nagata	$17^{\rm h}03^{\rm m}09^{\rm s}\!.908$	0.01	$17^{\rm h}03^{\rm m}10^{\rm s}\!.469$	0.007	0.561	4.444±0.055
11	H. Yoshihara	$17^{\rm h}03^{\rm m}30^{\rm s}\!.449$	0.011	$17^{\rm h}03^{\rm m}31^{\rm s}\!.005$		0.556	4.404
12	Yamamoto et al.	$17^{\rm h}03^{\rm m}22^{\rm s}\!.948$	0.033	$17^{\rm h}03^{\rm m}23^{\rm s}\!.612$	0.023	0.664	5.260±0.182
13	Ishiguro et al.	$17^{\rm h}04^{\rm m}33^{\rm s}\!.010$	0.022	$17^{\rm h}04^{\rm m}33^{\rm s}\!.735$	0.026	0.725	5.743±0.206
14	M. Ida	$17^{\rm h}03^{\rm m}09^{\rm s}\!.238$	0.011	$17^{\rm h}03^{\rm m}09^{\rm s}\!.976$	0.009	0.738	5.846±0.071
15†	H. Matsushita	$17^{\rm h}03^{\rm m}09^{\rm s}\!.15$	0.18	$17^{\rm h}03^{\rm m}09^{\rm s}\!.98$	0.18	0.83	6.575±1.426
16	Isobe et al.	$17^{\rm h}03^{\rm m}22^{\rm s}\!.874$	0.005	$17^{\rm h}03^{\rm m}23^{\rm s}\!.606$	0.005	0.732	5.798±0.040
17	Kitazaki et al.	$17^{\rm h}03^{\rm m}21^{\rm s}\!.199$	0.006	$17^{\rm h}03^{\rm m}21^{\rm s}\!.914$	0.007	0.715	5.664±0.055
18	H. Yamamura	$17^{\rm h}03^{\rm m}09^{\rm s}\!.474$	0.008	$17^{\rm h}03^{\rm m}10^{\rm s}\!.16$	0.008	0.686	5.434±0.063
19	Fujiwara et al.	$17^{\rm h}03^{\rm m}22^{\rm s}\!.862$	0.005	$17^{\rm h}03^{\rm m}23^{\rm s}\!.491$	0.006	0.629	4.982±0.048
20	Imamura et al.	$17^{\rm h}03^{\rm m}17^{\rm s}\!.324$	0.005	$17^{\rm h}03^{\rm m}17^{\rm s}\!.935$	0.005	0.611	4.840±0.055
21	Hi. Watanabe	$17^{\rm h}03^{\rm m}09^{\rm s}\!.504$	0.005	$17^{\rm h}03^{\rm m}09^{\rm s}\!.928$	0.005	0.424	3.359±0.040
22	H. Kasebe	$17^{\rm h}03^{\rm m}22^{\rm s}\!.635$	0.008	$17^{\rm h}03^{\rm m}23^{\rm s}\!.002$	0.006	0.367	2.907±0.048

*Length of chord was calculated as an approximate speed of the asteroid's shadow of 7.9212 [km s^{-1}] provided by IOTA's prediction (see table 1).

†Very large uncertainties; ignored in the reduction results.

by the dark blue vertical line in the graph, can be determined by finding a point on the graph where the pink dots line up in a straight line downward by selecting the point (red point) just before intersection of the line with the count value = 0 below and performing a linear approximation using the points before and after (blue points). Then, Limovie automatically calculates the average delay/advance of the timestamp relative to the time (UTC) of the measured 1 PPS LED emission, based on the starting position. This procedure was performed twice for the LED emissions taken before and after the observation, and then the average delay or advance of the timestamps was collected. Finally, time correction was applied to the acquired data by pressing the button "Apply to Analysis."

Next, the light curve of the target star was measured by Limovie. For photometry of these data, the radius of the aperture was set to 2, the inner radius of the sky was 4, and the outer radius of the sky was 17 pixels. After all the procedures mentioned above were completed, detailed prediction information (provided by Steve Preston; see section 2) was provided to Limovie, including the event date and time, the asteroid name, the target star name, the speed of Phaethon's shadow, and the distance to the asteroid. These were then reflected in the diffraction simulation described below.
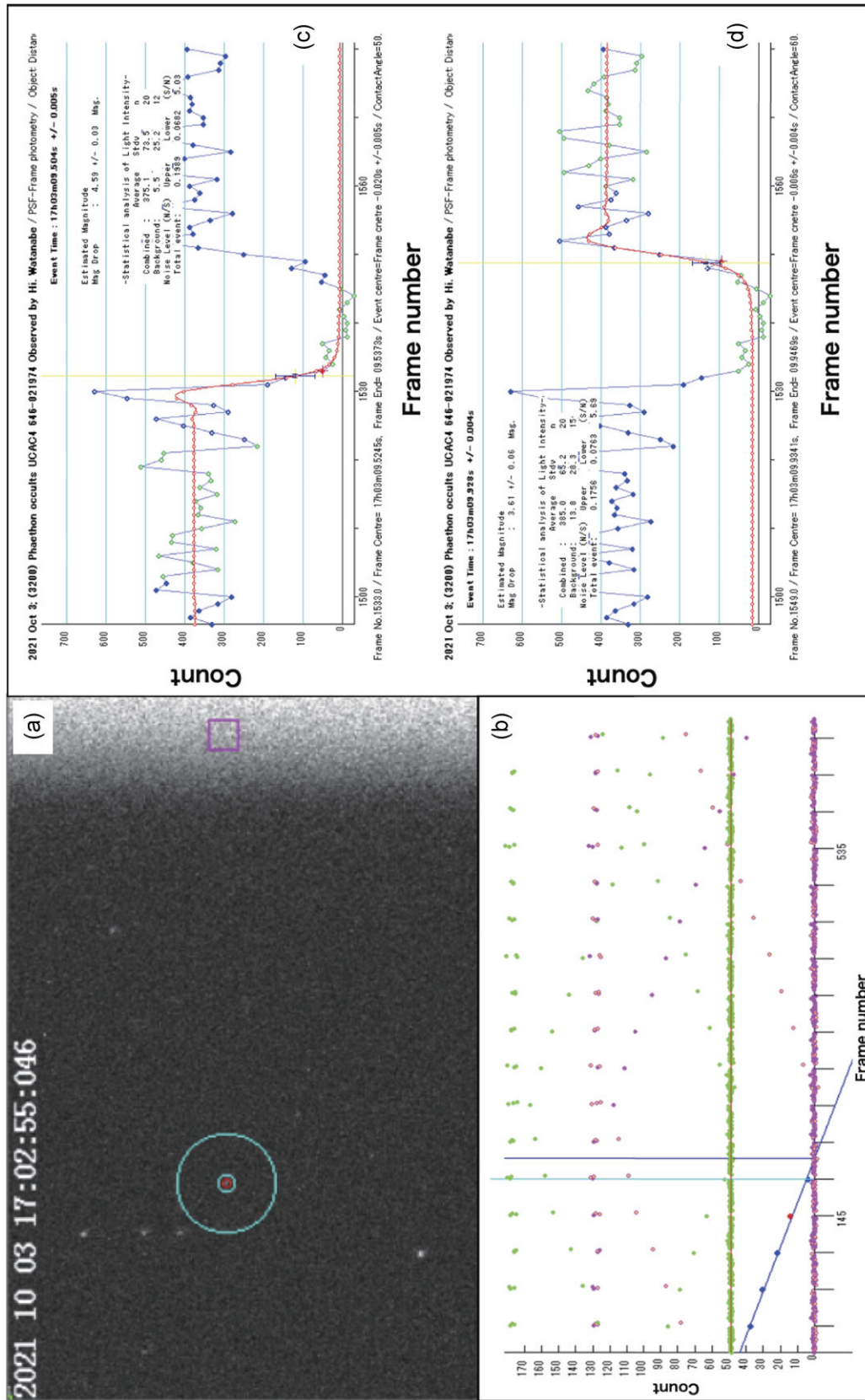
The light curve of the target star is shown by blue and green dots in figures 3c and 3d; the light curves of the target star in figures 3c and 3d are identical. The green dots in the light curve indicate regions that were averaged to obtain the brightness of the target star before and after disappearance.

The brightness of the target star does not fade instantaneously at the time of disappearance owing to light diffraction. In occultation observations, we generally compare the brightness of the target star during its appearance with that during its disappearance, and the time of disappearance is recorded when the brightness reaches a quarter of the brightness during its appearance. The time of emergence (reappearance) was defined in the same manner. The red curves in figures 3c and 3d are the regression light curves of the diffraction simulations based on the brightness before and after the disappearance (or appearance), distance to the asteroid, and speed of the asteroid's shadow. The yellow vertical lines in figures 3c and 3d represent the positions of disappearance (or appearance) determined from the graph. The horizontal error bar in the yellow line (the black error bar) is the uncertainty in the event time as estimated by Limovie, and the vertical error bar is the error in the amount of light. The frames that appear closest to these times are indicated by red filled circles in figures 3c and 3d.

In actual observations, the light intensity varies owing to atmospheric fluctuations and thermal noise in CMOS photodetectors; therefore, the light intensity measurements before and after a stellar occultation event are generally noisy. This noise can cause uncertainty during an event.

Fig. 3. Image and light curve of the target star during the occultation taken at observation site No. 21. (a) An image taken using SharpCap and displayed using Limovie. The star hidden by Phaethon is indicated by a red circle. The light blue concentric circles represent the sky background specified for photometry. (b) The graph used to measure the delay or advance of the timestamp relative to the PPS emission. The red circle indicates the frame closest to the time of the event selected by the analyst. The green circles show the light curve of the target star. The blue-circled curves in (c) and (d) show the light curve of the target star. The green circles show the region averaged to obtain representative values of the target star's brightness before and after occultation. The vertical yellow line represents the exact positions of the disappearance/appearance obtained from the light-diffraction simulation. See text for details.

However, simulations of noise (inverse of the signal-to-noise ratio) and time uncertainty have confirmed that the time of an event can be estimated with an uncertainty of a quarter or less of the exposure time of each frame in many cases of stellar occultation.

The same analysis was performed on the data from other observation sites to determine the time of disappearance and appearance. Figure 4 shows light-curve examples of time reading and time correction reported from each observation site. Observers used Limovie to accurately read the time of disappearance and appearance, corrected the times, and reported the corrected precise time of occultation. The results are shown in table 4, where at the appearance time of No. 11 and the observation sites of Nos. 6, 7, and 8, the LED emission of 1 PPS was not well recorded. Therefore, the disappearance and appearance time uncertainties for these observation sites are left blank in table 4. At these stations, the times were determined based on the accuracy of the preset computer system clocks.

The reduction was performed using the software "Occult4,"[12] which occultation observers widely use. Occult4 could calculate the size of Phaethon's shadow at any observation site based on the latitude, longitude, and elevation of the observation point; the time of disappearance and appearance observed at that point; and the speed of passage of Phaethon's shadow. By converting the latitude and longitude of each observation point to the x and y coordinates of a certain plane and displaying the length of the shadow observed there, the shape of Phaethon's shadow was obtained, as shown in figure 5. The numbers in figure 5 correspond to the numbers of the observation points in tables 3 and 4. The error bar at each point is the value obtained by converting the time uncertainty into chord length using the speed of Phaethon's shadow. The point marked "37" seen inside the ellipse in figure 5 is the prediction point of center of this event. The proximity of the prediction point to the center of Phaethon's shadow indicates that occultation occurred almost exactly as predicted, meaning that information about Phaethon's orbit and the coordinates of the star hidden by Phaethon were very accurate.

From this observation, the Phaethon cross-section at the time of stellar occultation by Phaethon on October 3 can be approximated by an ellipse with a major diameter of 6.12 ± 0.07 km and a minor diameter of 4.14 ± 0.07 km, position angle (PA) $117°.4 \pm 1°.5$. The uncertainty in the shadow length calculated from the time uncertainty of each observation point is 40–200 m. A large number of observers and a dense network of observations made it possible to determine not only the east–west size of Phaethon's shadow

but also the north–south limit with good accuracy. The success of this observation was due to several facts: (1) stellar occultation by Phaethon, which has been observed several times since 2019 (in the western USA on 2019 July 29; California, USA on 2019 September 29; Algeria on 2019 October 15 and 25; and Japan on 2019 October 15) made the prediction very accurate; (2) a call from the DESTINY$^+$ project brought together a large number of observers with appropriate equipment; (3) the occultation zone crossed western Japan widely, allowing for a wide and dense deployment of observers; and (4) the weather was very good on the day of observation, except in some areas.

## 5 Summary and future observation plans

In response to a request from the DESTINY$^+$ project team, we observed the asteroid (3200) Phaethon occulting a 12th magnitude star in the constellation Auriga: UCAC4 646−021974 = GSC 2894−00131. This event occurred on 2021 October 3 at 16:58 UTC along the path between Japan and Korea. 72 observers were distributed across 36 sites in and near the occultation zone. The star occulted by Phaethon disappeared at 18 observation sites; seven sites were outside Phaethon's shadow. From this observation, we determined Phaethon's cross-section at the time of stellar occultation, which can be approximated by an ellipse with a major diameter of 6.12 ± 0.07 km and a minor diameter of 4.14 ± 0.07 km, PA $117°.4 \pm 1°.5$. This shadow size was determined using an uncertainty of 40–200 m based on the time uncertainty of each observation point. In addition to the size in the east–west direction, the northern and southern limits of the shadow were also determined with good accuracy. This is the first time that an occultation event of a small asteroid with a diameter of 5 km has been observed with an accuracy of several tens of meters.

Although we observed only one cross-section of Phaethon in this campaign, there are many predicted stellar occultations by Phaethon before the DESTINY$^+$ flyby in 2028. Table 5 lists the occultation events of stars brighter than the 13th magnitude by Phaethon until flyby day. These predictions were made by Occult4 and should be updated with each perihelion passage of Phaethon.

Each stellar occultation provides a different cross-sectional view of Phaethon, thus providing useful data for further improving Phaethon's shape model. The DESTINY$^+$ science team will revise Phaethon's 3D shape model based on the results of this occultation observation, and a new shape model will be published in a separate paper.

The occultation observations were performed using a GPS module for accurate time information and a CMOS camera with high sensitivity, low noise, and high frame rate.

---

[12] ⟨http://www.lunar-occultations.com/iota/occult4.htm⟩.

No.16

No.17

No.20

No.22
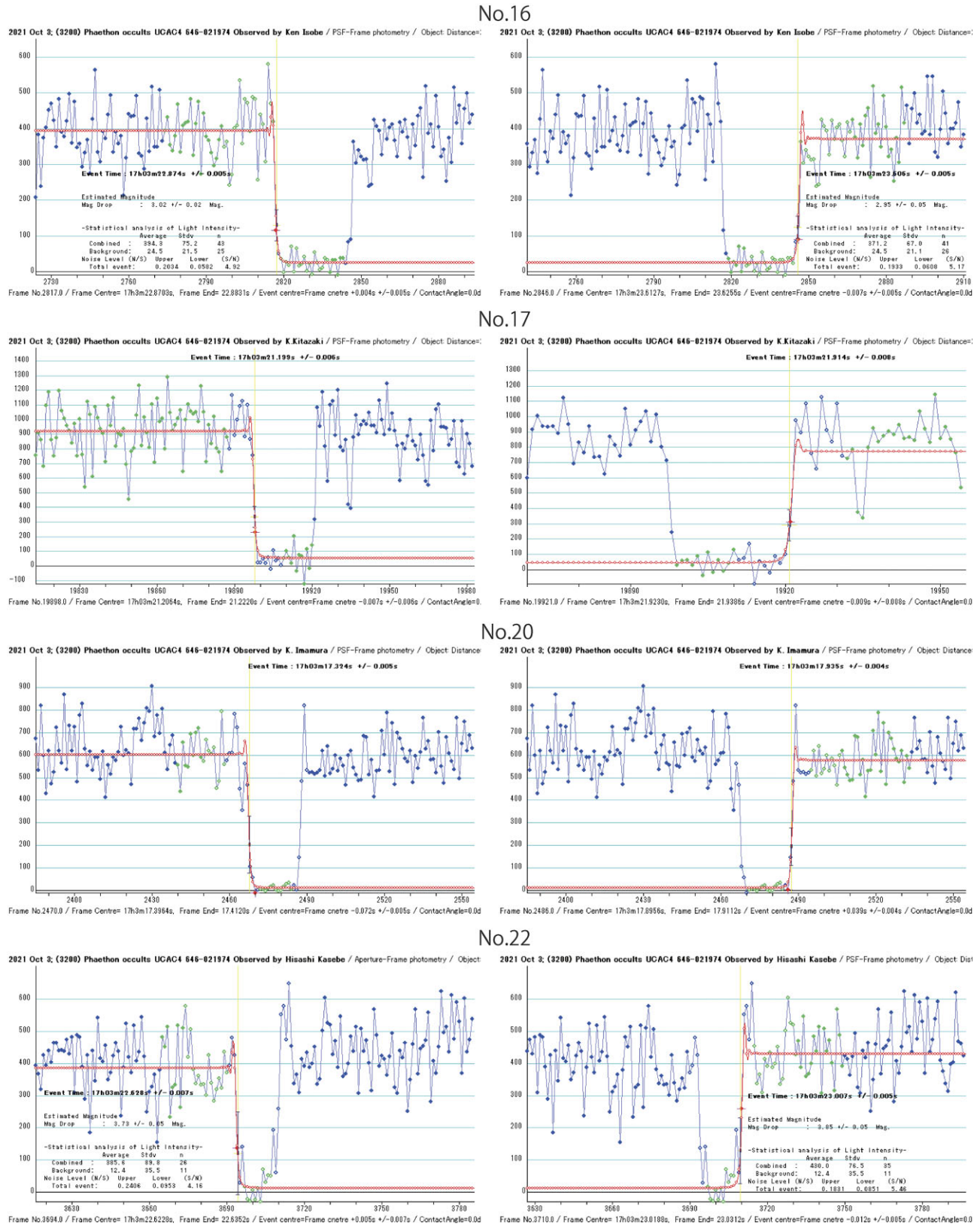
Fig. 4. Light-curve examples reported from each observation site. These figures are screen snapshots of the time readings and time correction light curves output by Limovie. At every site, observers used Limovie to accurately read the event time, correct the event time, and report the time of occultation. Here we present examples for sites 16, 17, 20, and 22 (see tables 3 and 4 for site numbers). These snapshots were collected from all sites, then used for the creation of a composite map like that shown in figure 5. The snapshots of the Limovie output include the observer's name, the time of disappearance and its frame number (left), and the time of reappearance and its frame number (right) in small letters. Depending on how the options are chosen, the measured magnitude drop, S/N, etc. can also be output together. Figures 3c and 3d also contain similar information. The disappearance and reappearance times output from each observation site by Limovie are shown in table 4.
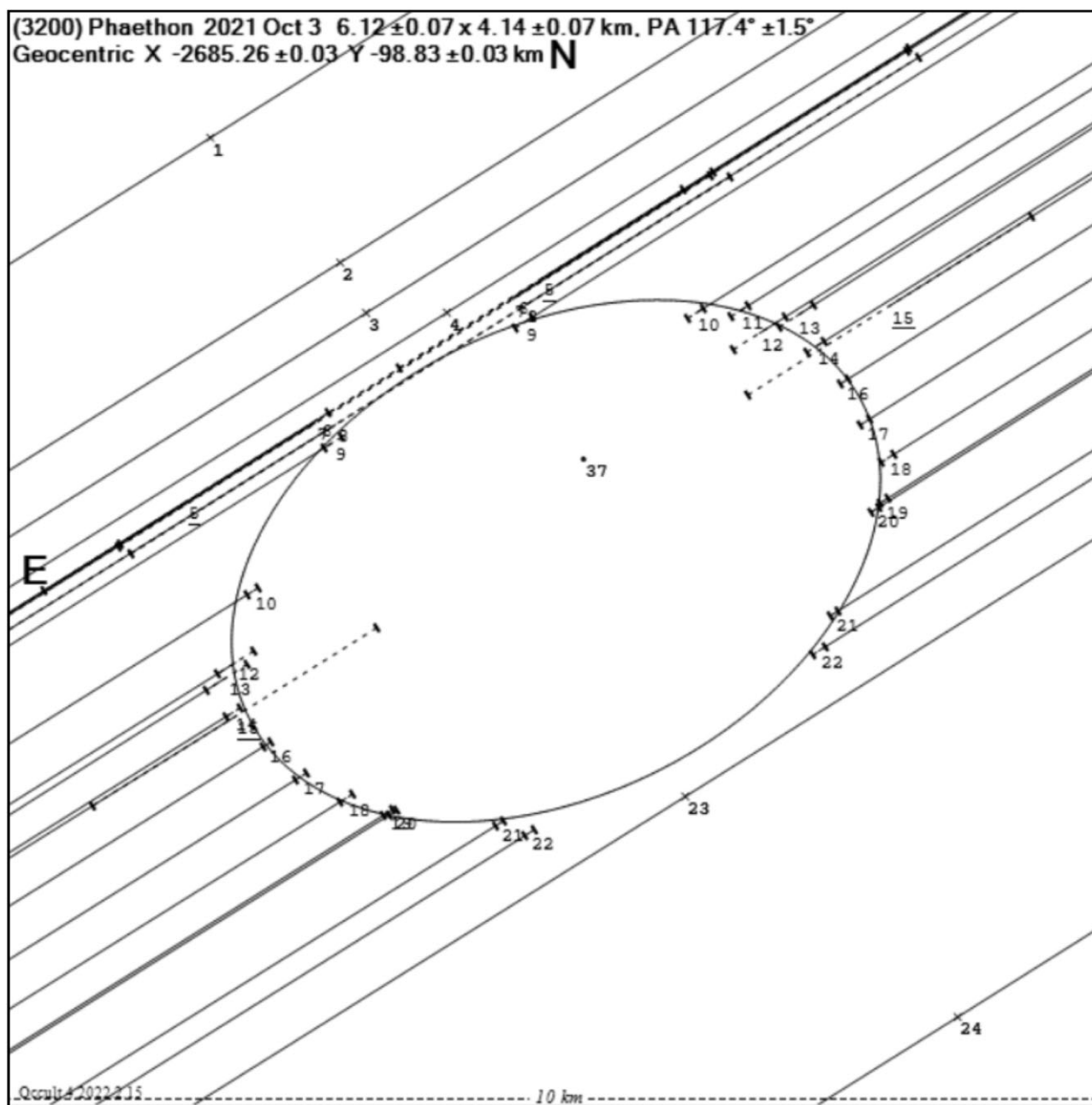
Fig. 5. Shadow shape of Phaethon reduced by Occult4. The numbers in the figure correspond to the numbers of observation sites listed in tables 3 and 4. The error bars associated with each point were calculated using the uncertainty of the time and the approximate speed of Phaethon's shadow (7.9212 km s^{-1}), which corresponds to 40–200 m. The observed chord was fitted with an ellipse with a major diameter of 6.12 ± 0.07 km and a minor diameter of 4.14 ± 0.07 km. The point marked "37" seen near the center of the ellipse is the prediction point of this event. The letters "N" and "E" written above and to the left of the figure indicate the directions of north and east, respectively. The scale is shown at the bottom of the figure, and the distance from the left end to the right end of the frame in the figure corresponds to 10 km. This figure shows that the observation points are densely located near the boundary of Phaethon's shadow, and not only in the major diameter of the ellipse but also in the minor diameter direction.

The combination of these instruments enabled observations with time resolutions several dozen times better than those of previous CCD-based observations. This will allow us to include fainter target stars and shorter-duration events in our observation list and to observe more occultation events.

Acknowledgments

Table 5. Stellar occultation events by Phaethon that will be visible in Japan until the Phaethon flyby by DESTINY[+].*

Date (UTC)	Time (UTC)	Star mag. (mag)	Max. duration (s)	Site
2022 Oct 5	11:53–12:05	12.8	0.27	E Japan
2022 Oct 21	14:27–14:36	10.8	0.22	Hokkaido
2022 Oct 22	18:51–19:00	12.8	0.22	W Japan
2023 Jan 10	08:08–08:28	11.3	0.48	Tohoku
2024 Nov 16	18:55–19:05	12.5	0.24	W Japan
2026 Oct 13	10:58–11:04	11.9	0.15	Tohoku
2026 Oct 17	09:45–09:52	11.0	0.16	Tokyo
2026 Oct 17	12:43–12:49	12.1	0.16	Hokkaido
2026 Oct 19	09:23–09:30	10.9	0.17	W Japan (Twilights)
2026 Oct 31	11:57–12:05	12.2	0.21	Hokkaido
2026 Nov 5	10:17–10:27	12.9	0.23	Kyushu
2027 Nov 17	14:00–14:23	11.5	0.54	Tohoku
2027 Nov 22	19:04–19:22	12.7	0.42	Kyushu
2027 Dec 2	13:00–13:12	11.4	0.29	Tohoku
2027 Dec 4	12:25–12:36	9.7	0.27	Tohoku
2027 Dec 6	18:24–18:35	11.4	0.25	Tokyo
2027 Dec 10	18:03–18:12	12.6	0.22	W Japan
2027 Dec 12	17:05–17:14	12.1	0.21	Hokkaido
2027 Dec 19	09:23–09:31	10.7	0.19	Japan
2027 Dec 20	16:37–16:45	9.1	0.19	Tohoku
2028 Jan 1	09:14–09:23	12.5	0.22	Japan

*Stellar occultations by Phaethon seen around the world should be published on the IOTA page ⟨https://www.asteroidoccultation.com⟩.

References

Ansdell, M., Meech, K. J., Hainaut, O., Buie, M. W., Kaluna, H., Bauer, J., & Dundon, L. 2014, ApJ, 793, 50

[13] ⟨DOI:10.26093/cds/vizier⟩.

Arai, T. 2021, in Proc. European Planetary Science Congress (Strasbourg: Europlanet Society), EPSC2021-877
Arai, T., et al. 2021a, LPI Contrib., 1896
Arai, T., Yamamoto, T., Ozaki, N., Toyota, H., Nishiyama, K., & Takashima, T. 2021b, Abstract, 43rd COSPAR Scientific Assembly, B1.1-0014-21, 276
Borisov, G., et al. 2018, MNRAS, 480, L131
Drake, A. J., et al. 2009, ApJ, 696, 870
Dunham, D. W., Dunham, J. B., Buie, M., Preston, S., Herald, D., & Farnocchia, D. 2019, LPI Contrib., 2189, 2062
Dunham, D., et al. 2020, BAAS, 52, 412.01
Dunham, D., et al. 2021, in Proc. 7th IAA Planetary Defense Conference (Vienna: United Nations Office for Outer Space Affairs), 37
Enos, H. L., & Lauretta, D. S. 2019, Nature Astron., 3, 363
Gaia Collaboration 2016, A&A, 595, A2
Gaia Collaboration 2018, A&A, 616, A1
Gaia Collaboration 2021, A&A, 650, C3
Gustafson, B. A. S. 1989, A&A, 225, 533
Hanuš, J., et al. 2016, A&A, 586, A108
Hanuš, J., et al. 2018, A&A, 620, L8
Hong, P., et al. 2021, LPI Contrib., 1741
Ishibashi, K., et al. 2021, LPI Contrib., 1405
Jenniskens, P. 2006, Meteor Showers and their Parent Comets (Cambridge: Cambridge University Press)
Jewitt, D., & Li, J. 2010, AJ, 140, 1519
Jewitt, D., Asmus, D., Yang, B., & Li, J. 2019, AJ, 157, 193
Kareta, T., Reddy, V., Hergenrother, C., Lauretta, D. S., Arai, T., Takir, D., Sanchez, J., & Hanuš, J. 2018, AJ, 156, 287
Kim, M.-J., et al. 2018, A&A, 619, A123
Krüger, H. 2021, in Proc. European Planetary Science Congress (Strasbourg: Europlanet Society), EPSC2021-871
Krugly, Y. N., et al. 2002, Icarus, 158, 294
Lauretta, D. S., et al. 2019, Nature, 568, 55
Lazzarin, M., Petropoulou, V., Bertini, I., La Forgia, F., Ochner, P., Migliorini, A., & Siviero, A. 2019, Planet. Space Sci., 165, 115
Lee, H.-J., et al. 2019, Planet. Space Sci., 165, 296
Li, Y., et al. 2021, Abstract, 43rd COSPAR Scientific Assembly, B1.1-0014-21, 307
Lin, Z.-Y., et al. 2020, Planet. Space Sci., 194, 105114
MacLennan, E., Toliou, A., & Granvik, M. 2021, Icarus, 366, 114535
Magnier, E. A., et al. 2020, ApJS, 251, 3
Ochsenbein, F., Bauer, P., & Marcout, J. 2000, A&AS, 143, 23
Ohtsuka, K., Sekiguchi, T., Kinoshita, D., Watanabe, J.-I., Ito, T., Arakida, H., & Kasuga, T. 2006, A&A, 450, L25
Ohtsuka, K., Nakato, A., Nakamura, T., Kinoshita, D., Ito, T., Yoshikawa, M., & Hasegawa, S. 2009, PASJ, 61, 1375
Ohtsuka, K., et al. 2020, Planet. Space Sci., 191, 104940
Pravec, P., Wolf, M., & Šarounová, L. 1998, Icarus, 136, 124
Tabeshian, M., Wiegert, P., Ye, Q., Hui, M.-T., Gao, X., & Tan, H. 2019, AJ, 158, 30
Taylor, P. A., et al. 2019, Planet. Space Sci., 167, 1
Watanabe, S., Tsuda, Y., Yoshikawa, M., Tanaka, S., Saiki, T., & Nakazawa, S. 2017, Space Sci. Rev., 208, 3
Watanabe, S., et al. 2019, Science, 364, 268
Williams, I. P., & Wu, Z. 1993, MNRAS, 262, 231